Tailoring the Activation Energy and the Ionic Properties of Bismuth co-doped SDC Powder Prepared by Solid State Reaction Method

Sandhya Kottooli (sandhyakprabeesh@gmail.com)
Govt.College for women https://orcid.org/0000-0003-3415-8212
N.S. Chitra Priya
Govt.College for Women,Trivandrum
J.S. Revathy
Govt.College for Women,Trivandrum
Deepthi N. Rajendran
Govt.College for Women
T. Praveen
E.S.P.R.T Industries Redon France

Research Article

Keywords: Solid state method, Dielectric studies, Impedance and Modulus spectroscopy

Posted Date: February 23rd, 2021

DOI: https://doi.org/10.21203/rs.3.rs-236828/v1

Version of Record: A version of this preprint was published at Journal of Materials Science: Materials in Electronics on April 8th, 2021. See the published version at https://doi.org/10.1007/s10854-021-05846-1.

Abstract

Research on fuel cell components has received great attention owing to the growing need for sustainable energy sources. Bismuth (Bi 3+) co-doped samarium doped cerium oxide [Ce 1-x Sm x-y Bi y O 2-δ (x=0.2 and y=0, 0.05 and 0.1)] nanosystems were prepared by solid state reaction method. Rietveld structure refinement of X-ray diffraction pattern confirms the cubic fluorite structure along the (111) plane with the decrease in lattice distortion. At the same sintering temperature, pellets exhibit good morphology with better mechanical strength. The conductivity measurements carried out using the Nyquist plot, as well as the modulus spectra, indicate the effect of grain and grain boundary conduction at high temperatures. With the increase in the incorporation of Bi dopant, there is a gradual decrease in ionic conductivity and activation energy. The composition of Ce 0.8 Sm 0.1 Bi 0.1 O 2-δ exhibits less ionic conductivity compared to other samples due to the oxygen vacancies attracted by dopant cations. The effect of Bi 3+ dopants on samarium doped ceria lattice structures and the electrical properties of the systems has been discussed.

1. Introduction

The rapid industrialization and urbanization increased the usage of energy in day-to-day life. The main crisis that we are facing is the massive discharge of contaminants and pollutants due to the heat engines utilizing fossil fuel. All these factors boost the prospect of global warming [1]. In this scenario, renewable energy technology has been considered one of the most appealing options for the survival of humankind. The fuel cell is regarded as the best candidate for energy conversion [2].

The researchers are focusing their attention on the solid oxide fuel cell (SOFC), due to their high energy conversion and low environmental impact. Yttria-Stabilized Zirconia (YSZ) was one of the most used electrolytes in high-temperature SOFCs. The high sintering temperature restricts its application in the SOFC applications[3]. Literature review reports samarium doped ceria (SDC) exhibit superior oxygen ion conductivity compared to YSZ electrolyte at intermediate temperature. The main drawback of SDC prepared by a solid state method is its high sintering temperature to obtain desirable chemical homogeneity and density. The pellet sintered at a high temperature cannot be easily cofired with the electrode material. To overcome these inherent limitations, it is desirable to prepare a high-density pellet at reduced sintering temperature to reduce the cost of fabricating SOFCs [4-6].

Bismuth oxide systems possess high oxide ion conductivity to make them the best suitable candidate for good electrolyte material. There are certain drawbacks for bismuth oxide systems and doped bismuth oxide systems which limits its application as an alternative electrolyte material. Doped Bismuth oxide systems possess a complex array of structures and their properties can be varied by changing the dopant concentration, temperature, and atmosphere. δ-Bi_2O_3 can be stabilized at room temperature by doping with smaller sized rare earth and/or donor dopant cations. The rare earth elements such as Gd, Ho, Nd, Sm, Y, Dy, Er, and higher valency cations such as W or Nb are used as dopants for Bi_2O_3 [7-10]. Biesuz et al reported that samarium doped ceria (SDC) were prepared and sintered at a temperature of ~ 500^oC.

The sintered pellet exhibits nanometric grain size with relatively high density [11]. Karaca et al worked on the preparation of nanocrystalline samarium doped CeO_2 by modified sol-gel process and hydrothermal content treatment and obtained ultrafine grain at the sintering temperature of 1300 ^oC [12].M.Prekasji et al reported that the highest ionic conductivity for bulk and grain boundary to be $3.14x10^{-3}$and $9.32x10^{-4}$ Scm^{-1} respectively at 700 ^oC for $Ce_{0.8}Bi_{0.2}O_{2-\delta}$ composition sintered using microwave (MS) sintering technique [13]. Accadro et al investigated the microstructure of the gadolinium doped ceria electrolyte, materials codoped ceria with bismuth oxide (1-5 mol%). The study reveals that high ionic conductivity was reported for the optimal 3% composition of bismuth [14]. Zhao et al studied the impact of the incorporation of a small amount of Bi_2O_3 to SDC prepared by Pechini-type gel routine. The analysis concluded that Bi^{3+} dopant plays a significant role in the anion transport of the materials [15]. Different preparation methods like solid-state reaction [16], solution combustion [17], citrate gel [18], and hydrothermal process [19] are used for synthesizing SDC nanopowder. The nanocrystalline materials exhibit better electrochemical properties like rapid densification kinetics, lower sintering temperatures, etc. Synthesizing electrolytes in nanoscale may result in improved performance of the cell. A detailed analysis of the ionic conductivity of the nanoscale material is to be explored. In this work, solid state reaction is used to prepare bismuth codoped SDC electrolyte, since it is a simple and inexpensive method.

In this work, attempts are made to investigate the effect of doping the trivalent bismuth ion on the SDC electrolyte. Co-doping SDC with trivalent ion tends to reduce the sintering temperature without compromising the ionic conductivity. A detailed study on ionic transport helps to tailor the material for desired applications.

2. Experimental Method

Bismuth-doped SDC electrolyte (BiSDC 5 and BiSDC 10) samples of varying concentrations of the dopant were processed using the solid state reaction method. For the solid state synthesis method, the stoichiometric amount of cerium oxide (CeO_2), samarium oxide (Sm_2O_3), and bismuth oxide (Bi_2O_3) were mixed and grinded using acetone as a solvent for 48 h in an agate mortar. After the grinding process, the powders were calcined at 600 ^oC for 2 h. The powders were uniaxially pressed by applying a pressure of 2.5 MPa in a cylindrical mold. Each pressed pellet was sintered at the same temperature 800 ^oC for 10 h. There was a shrink in the diameter of the pellets after the sintering process. Different dopant concentration was studied to determine the change in the ionic conductivity of the doped material. The electrical measurements of the sintered pellets were performed using an Impedance analyzer, Solatron 1260A

3. Results And Discussion

3.1.XRD STUDIES

The Rietveld simulated X-ray diffractograms of Bismuth doped ceria lattice is shown in Fig.1. After the calcination process, the XRD pattern gives a clear indication of the cubic fluorite structure (ICCD file no:34-0394). This structure is more suitable as an ionic conductor and is related to cerium oxide. Scherrer equation is used to calculate the average crystallite size [20] and the computed lattice parameter, volume, and density of the sample obtained from refinement are listed in Table.1. From the reported literature, it is understood that the ionic conductivity of oxides is mainly affected by the degree of lattice distortion [21]. The degree of lattice distortion depends on the discrepancy in the ionic radii of the host lattice and dopant cations. The crystallite size reached the nanometric range with the addition of dopants.

Table 1: demonstrates Lattice parameters, Crystallite size, Volume, Good of fit goodness of fit (Chi^2) obtained after Rietveld refinement

Composition	Lattice parameter Å	Crystallite size unit (nm)	Volume $V((Å)^3)$	Chi^2
$Ce_{0.8}Sm_{0.2}O_{2-\delta}$	5.44337	21	161.288	2.48
$Ce_{0.8}Sm_{0.15}Bi_{0.05}O_{2-\delta}$	5.41498	19	158.778	1.49
$Ce_{0.8}Sm_{0.05}Bi_{0.15}O_{2-\delta}$	5.39811	15	157.299	1.42

The Fig.2. shows the morphology of SDC, BiSDC 5, and BiSDC 10 pellets sintered at 800 ^oC for 10 h. The morphology of the SDC pellets sintered at 800 ^oC for 10 h indicates, separately, the grains and grain boundaries. It is noted that on the BiSDC 5 and BiSDC 10 sample surface, the nanopowders are agglomerated in the form of clusters. As the size of the cluster become bigger, the densification of the electrolyte gets retarded. This demonstrates the incorporation of Bi in SDC lattice supports the generation of clusters on precursor material.

3.3. Dielectric Studies

Fig.3 shows the disparity of loss tangent(tanδ) with frequency for different concentrations of the dopants. There is a decline in loss tangent(tanδ) value with the increasing frequency in all samples owing to the mobile ion charge carriers. At higher frequency, the loss tangent parameter becomes almost frequency- independent in all samples. At higher temperatures, an increase in tanδ is observed which contributes to the high ionic conductivity in the material. It is noted that at a higher temperature in all samples, there is a sudden rise in loss tangent at the low frequency region owing to the space charge polarization [22].

3.4. Electrical Studies

Fig.4 shows the disparity of the imaginary part of impedance with the change in frequency at a selected temperature. It is noted that each plot contains a relaxation peak at higher frequencies related to bulk conduction. As the temperature increases, the peaks are found to be deviating towards the higher frequency side. The same behavior is exhibited for both the sample. The change in the peak frequency with a temperature rise obeys the Arrhenius relation [23].

Fig.5 illustrates the Nyquist plot of the Bi-doped SDC observed at a different temperature. From the graph, as the temperature increases, there is the relative contribution of Grain Interior (GI) and Grain Boundary (GB). The ionic conductivity is observed to be low at a lower temperature due to the increase in the GI resistance contribution in all samples. As the temperature increases, there is a monotonically decrease in impedance in GI due to the dissolution of some Bi_2O_3 into the cubic lattice of the SDC structures. The decrease in GI impedance is attributed to a charge transfer reaction in which oxygen is evolved at the electrode-electrolyte interface [24].

The ionic conductivity of the prepared pellet sintered at the same temperature in the air with a temperature change is shown in Fig.6. As can be seen, the ionic conductivity of the prepared pellet at a higher temperature under study. The total conductivity is screened in the form of an Arrhenius plot. There is a change in the slope of the Arrhenius plot for different concentrations of the dopants Bi^{3+} and Y^{3+} at a higher temperature of 750 ^oC. So, the Arrhenius plot is divided into two parts one at low temperature and another at high temperature regime related to different activation energies. The literature report Bi^{3+} is highly polarizable due to the existence of $6s^2$ lone pair of electrons. The presence of $6s^2$ lone pair of electrons helps them to incorporate into the relatively disordered surroundings. Wachsman et al. [29-30], reported that the oxygen ion transport mechanism involves the migration of oxygen ions from regular 8c sites to interstitial 32f sites. Thus, the migration of oxygen ions give support to Bi_2O_3 segregation at the grain boundaries and enhances the oxygen ion conductivity. Electrical studies show greater ionic conductivity for samarium doped ceria with an increased amount of samarium due to the less deformation in the ceria lattice. This is mainly due to the ionic radius of samarium near that of host ion ceria (Ce^{4+}). But the ionic conductivity of the $Ce_{0.8}Sm_{0.1}Bi_{0.1}O_{2-\delta}$ was found to be lower than $Ce_{0.8}Sm_{0.15}Bi_{0.05}O_{2-\delta}$ and $Ce_{0.8}Sm_{0.2}O_{2-\delta}$. As the amount of Bi^{3+} dopant increases, the oversized Bi^{3+} produces a strong distortion in the ceria lattice. There is a decrease in grain boundary mobility due to the oxygen vacancies attracted by the dopant cations. This effect does not show a linear relationship and is constrained to a certain doping percentage [15]. The total ionic conductivity of the samples is tabulated and given in table 2.

Compositions	Activation energy E_a(eV) Low High temp temp	Conductivity (Scm^{-1}) at 750°C at 1MHz
$Ce_{0.8}Sm_{0.2}O_{2-\delta}$	0.16 0.66	$7.96x10^{-05}$
$Ce_{0.8}Sm_{0.15}Bi_{0.05}O_{2-\delta}$	0.06 0.71	$1.75x10^{-05}$
$Ce_{0.8}Sm_{0.05}Bi_{0.15}O_{2-\delta}$	0.05 0.58	$6.60x10^{-06}$

3.5. Modulus spectroscopy

Modulus spectroscopy technique is one of the most powerful tools to determine electrical inhomogeneity and carriers transport mechanism in electrolytes. Modulus formalism helps in suppressing electrode effect and dominating the bulk effects on the frequency domain. The complex modulus spectra are usually obtained from the impedance using the relation.

$$M^* = M' + iM'' = i\omega C_0 Z^* \qquad (1)$$

Where $\omega=2\Pi f$ is the angular frequency, $i=\sqrt{-1}$, $C_0= \varepsilon_0 S/d$ is the empty cell capacitance, ε_0 is the absolute permittivity, S is the surface area and d is the thickness of the sample. Fig. 7 shows the disparity of M' with frequency in the temperature range 200-500 °C. There is a change in the value of M' for both low and high frequencies. In the low frequency region, very low of M' is noted in all the samples. But as the temperature varies there is a steady rise in the dispersion as frequency changes from 1Hz to 1Mhz. This is a clear indication of lacking restoring force controlling the mobility of the charge carriers [31]. From the observation, it is evident that there is no electrode effect in the samples shown in Fig. 7. Fig.8 shows the disparity of M" with frequency in the temperature range 200-500 °C. There is a deviation in the relaxation peak towards the higher frequency sides in all samples which reveals the existence of hopping of carriers in all the samples [32].

4. Conclusion

The bismuth codoped SDC samples were processed by the solid state reaction method. XRD images show the cubic fluorite structure with high intensity along the (111) plane. A difference in surface morphology is noted for the codoped samples at the same sintering temperature due to the varying concentration of Bi_2O_3. It is noted that there is a reduction in dissipation factor with the rise in frequency. The grain and grain boundary resistance decrease with a rise in temperature from the Nyquist plot in all the co-doped samples. The total ionic conductivity and activation energy are obtained from the Arrhenius plot at the temperature of 400-750 °C. At higher temperatures, the activation energies are noted to be less

than 1 eV in all the samples. This work provides an insight that the varying concentration of the dopants has a great impact on the ionic conductivity of the bismuth co-doped SDC electrolyte.

Declarations

Acknowledgment

Sandhya K and Chitra Priya N S would like to express sincere thanks to University of Kerala for their financial support in the form of fellowships. Revathy J S wishes to thank the Department of Science and Technology (DST), INSPIRE fellowship, Govt. of India, for financial assistance [Grant No. IF160231]. The authors thank NIIST Trivandrum, STIC Cochin and Dept. of Chemistry, Govt. College for Women, Thiruvananthapuram, Kerala for the provision of characterization facilities.

References

[1]. Steel BCH and A.Henizel , *Nature*. **414** 345(2001)

[2]. E.D. Wachsman and K.T. Lee, *Science.* **334** 935(2011)

[3]. S.Omar, E.D.Wachsman, J.L. Jones and J.C. Nino *J. Am. Ceram. Soc.* **92** 2674 (2009)

[4]. L.Blum, *Int.J. Appl.ceram.Technol.***2** 1 *(2005)*

[5]. J.Y. Park, H .Yoon and E.D.Wachsman *J.Am.Ceram.Soc.* **88** 2402 (2005)

[6]. L.D. Jadhav, S. H. Pawar and M.G. Chourashiya, *Bull. Mater. Sci.***30** 97 (2007)

[7]. T.Takahashi, Y.Iwahara Hagia *J. ppl. Electrochem.***2** 97 (1972)

[8]. H.Kruidhof, *Solid State Ionics***50** 181 (1992)

[9]. Shuk H, *Solid State Ionics***89** 179 (1996)

[10]. N.Jiang, E.D.Wachsman, S. Jung *Solid State Ionics***150** 347 (2002)

[11].Mattia Biesuz, Luca Spiridigliozzi , Matteo Frasnelli, Gianfranco Dell'Agli and M Vincenzo,*Mater.Lett.* **190** 17 (2017)

[12].Tuba Karaca, Tuba Gürkaynak, M Altınçekiç, Faruk Öksüzömer, *Ceram. Int.* **36** 1101 (2010)

[13]. M. Prekajski, M.Stojmenvic, A.Radojkovic, G.Brankovic, H.Oraon**,** R.Subasri and B Matovic J. *of Alloys and Compounds***617** 563 (2014)

[14]. G.Accardo, D.Frattini, H.C. Ham, J. H. Han and S.P. Yoon *Ceram. Int.* **11** 165(2017)

[15]. Wenguang Zhao, Shengli An, and Liang Ma , *J. Am. Ceram. Soc.***94** 1496 (2011)

[16]. R.Punn, A.M. Feteira, D.C. Sinclair and C Greaves, *J.Am.Ceram.Soc.***128** 15386 (2006)

[17]. T. S. Zhang, J.Ma, H.Cheng and S.H. Chan. Mater. Res. Bullet. **41** 563 (2006)

[18]. S.Boskovic, S.Zec, J.Dukic, D.Bucevac and B. Matovic *NANO***33** 43 (2011)

[19]. D.Ivanova, A.Kovalevsk, V. V. Kharton, F.M.B Marques , *Bol. Soc. esp. Ceram. V.* **47** 201(2008)

[20]. Leow Chun Yan, and Jumian Hassan,*World Appl.Sci. J.***14** 1091 (2011)

[21]. A.I.Y Tok, F.Y. C Boey, Z.Dong and X.L. Sun *Journal of Materials Processing Tech.***190** 217 (2007)

[22]. Pandurangan Muralitharan, Seung Hwan Jo and Do Kyung Kim, *J. Am. Ceram. Soc.***91** 3267 (2008)

[23]. Vaisakhan Thampi, Prabhakar Rao Padalaand and A.N Radhakrishnan, *New J. Chem.***39** 1469 (2015)

[24]. L.B. Mc Cusker, R.B. Von Dreele, D.E. Cox, D.Louer and P.Scardi, *J. Appl. Crystallogr.***32** 36 (1999)

[25]. J.Kimpton , T.H. Randle and Drennan , *J. Solid State Ionics.***149** 89 (2002)

[26]. M.J. D Rushton and A.Chroneos,*Sci Rep.* **4** 6068 (2014)

[27]. J.A. Kilner, *Solid State Ionics.* **129** 13 (2000)

[28].S. Ramesh, V. P. Kumar, P. Kistaiah and C.V. Reddy *Solid State Ionics* **181** 86 (2010)

[29]. C. Kjølseth, H .Fjeld, Ø. Prytz, P.Inge, C.Estournès, R.Haugsrud and T .Norby ,*Solid State Ionics*. **181** 268 (2010)

[30]. K. T. Lee, A. A. Lidie, S. Y. Jeon, G. T. Hitz, S. J. Song and E. D.Wachsman, 2013 *J. Mater. Chem.* A. **1** 6199

[31]. N. M. Sammes, G.A. Tompsett, H.Näfe and F.Aldinger *J. Eur. Ceram. Soc.***19** 1801 (1999)

[32]. E. D. Wachsman, S.Boyapati, M. J. Kaufman and N.Jiang , *J. Am. Ceram. Soc.***83** 1964 (2004)

Figures

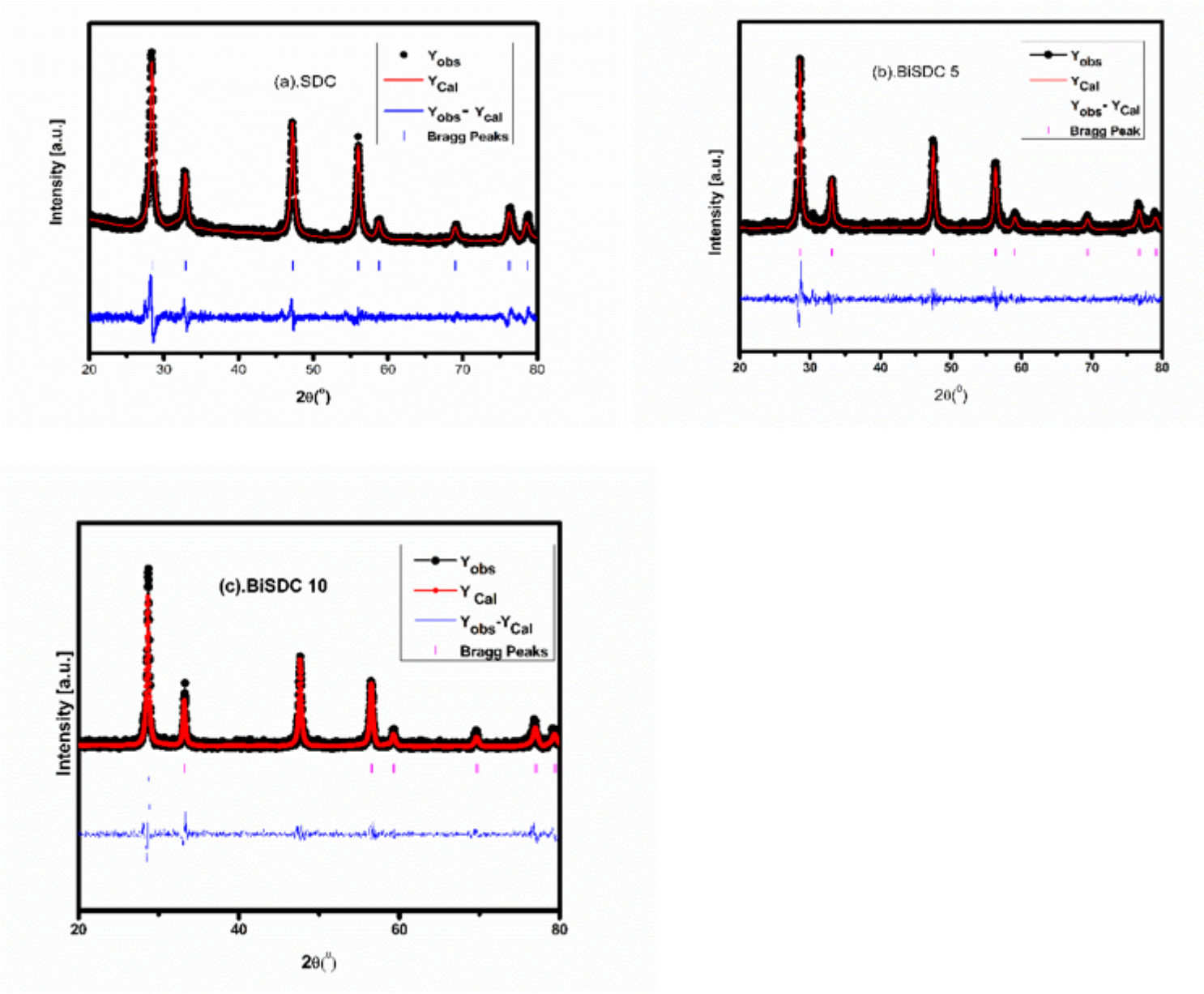

Figure 1

The Reitveld refinement XRD pattern of 1(a).SDC, 1(b).BiSDC 5and 1(c).BiSDC 10 samples.

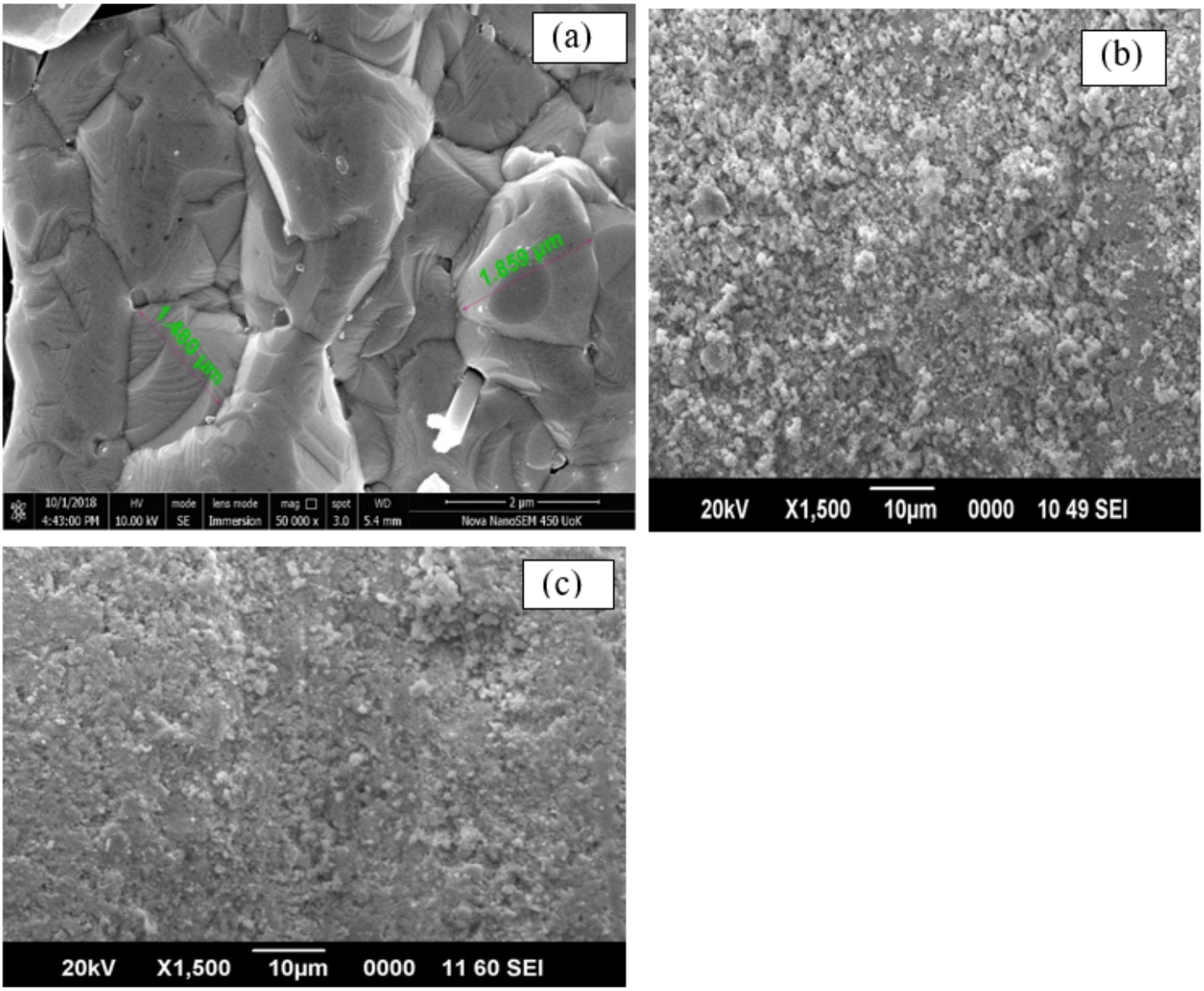

Figure 2

SEM images of 2(a) SDC, 2(b) BiSDC 5 and 2(c) BiSDC 10 samples.

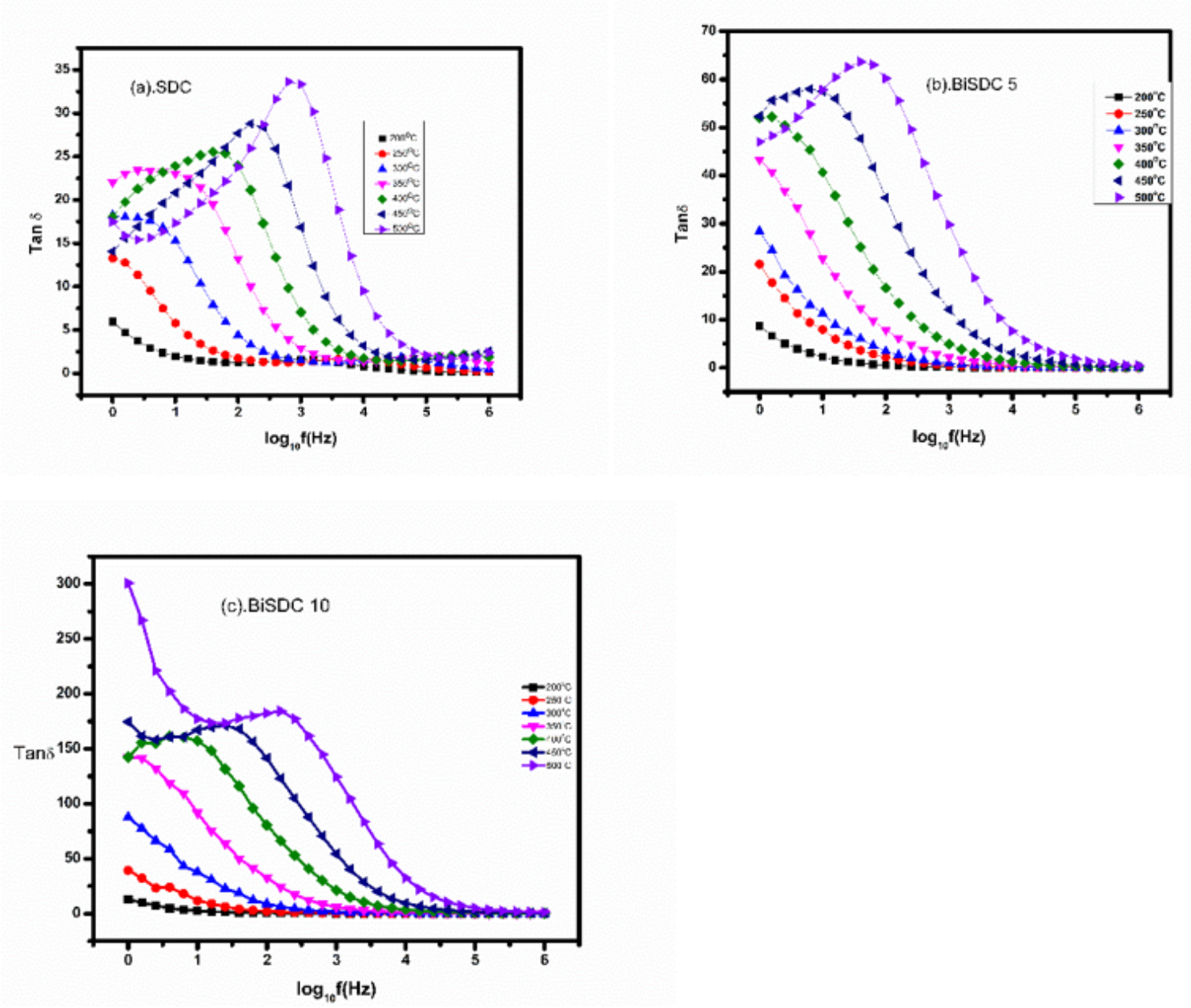

Figure 3

Shows variation of loss tangent with frequency at temperature 400-550oc 3(a).SDC 3(b).BiSDC 5 and 3(c). BiSDC 10 samples.

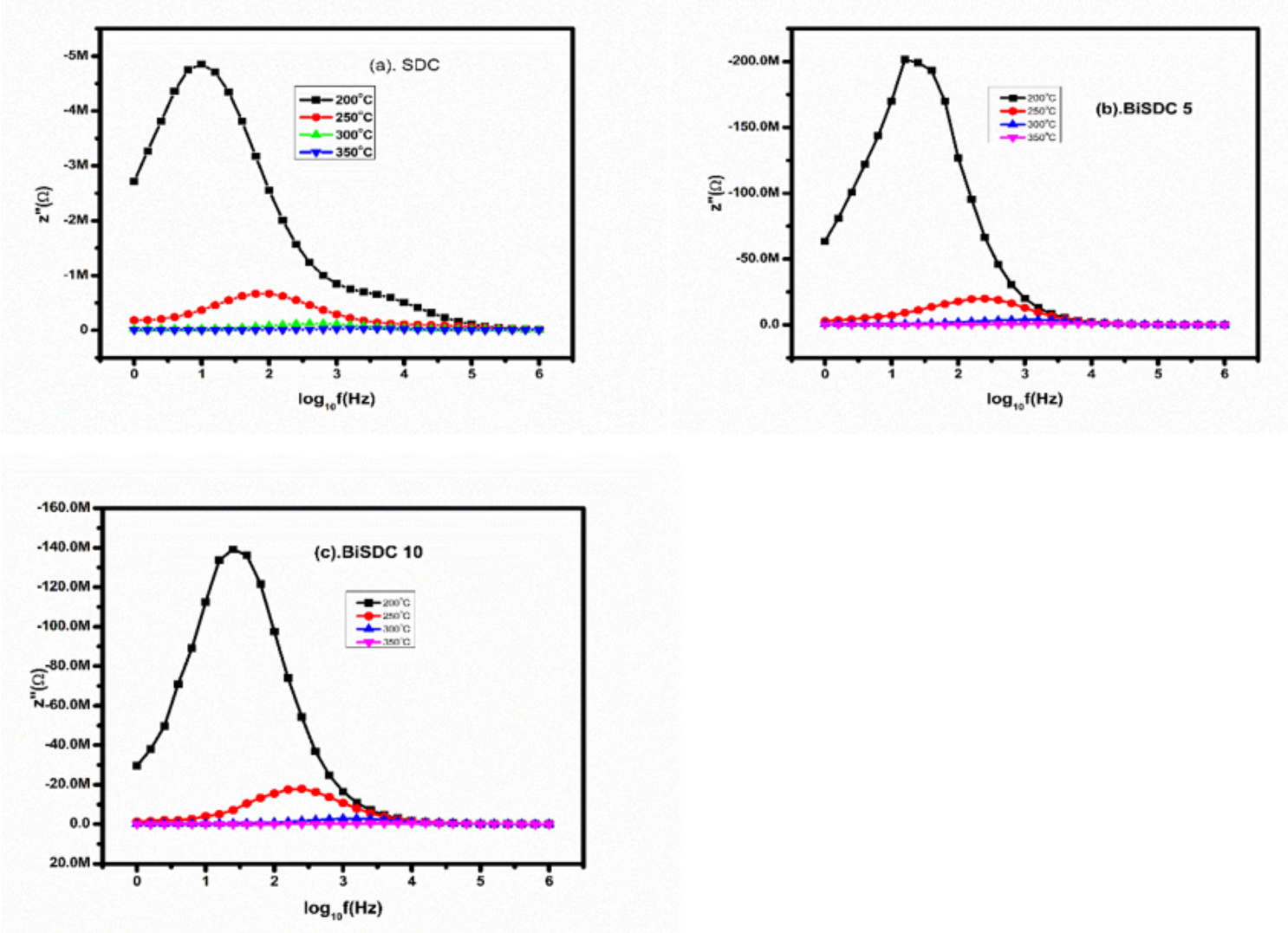

Figure 4

shows the disparity of the imaginary part of impedance with frequency at selected temperature 200-325oC 4(a)SDC, 4(b)BiSDC 5, and 4(c) BiSDC 10samples

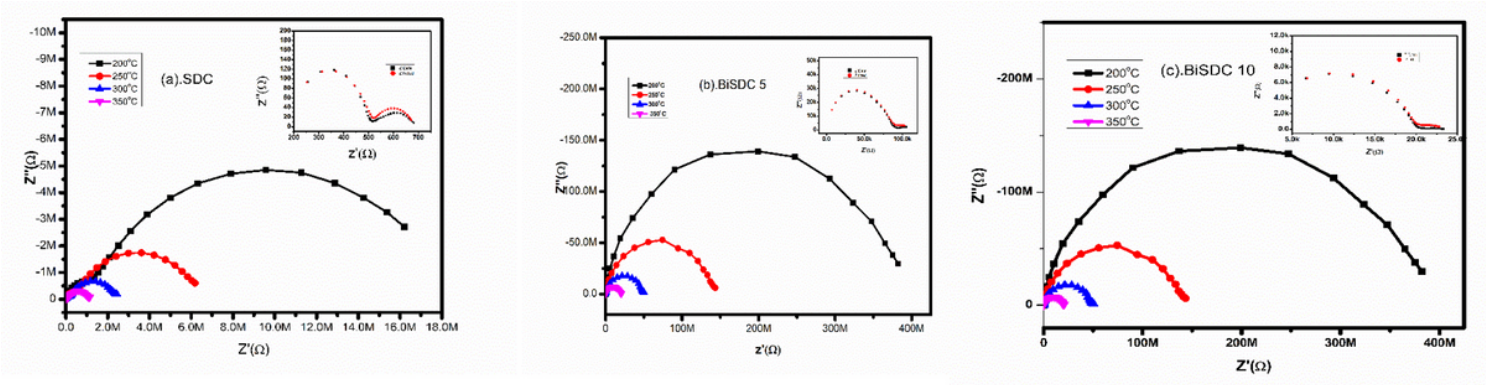

Figure 5

Nyquist plot of 5(a)SDC 5(b) BiSDC 5 and 5(c)BiSDC 10 at 400oC in the inset of fitted Nyquist plot fitted at 600oC.

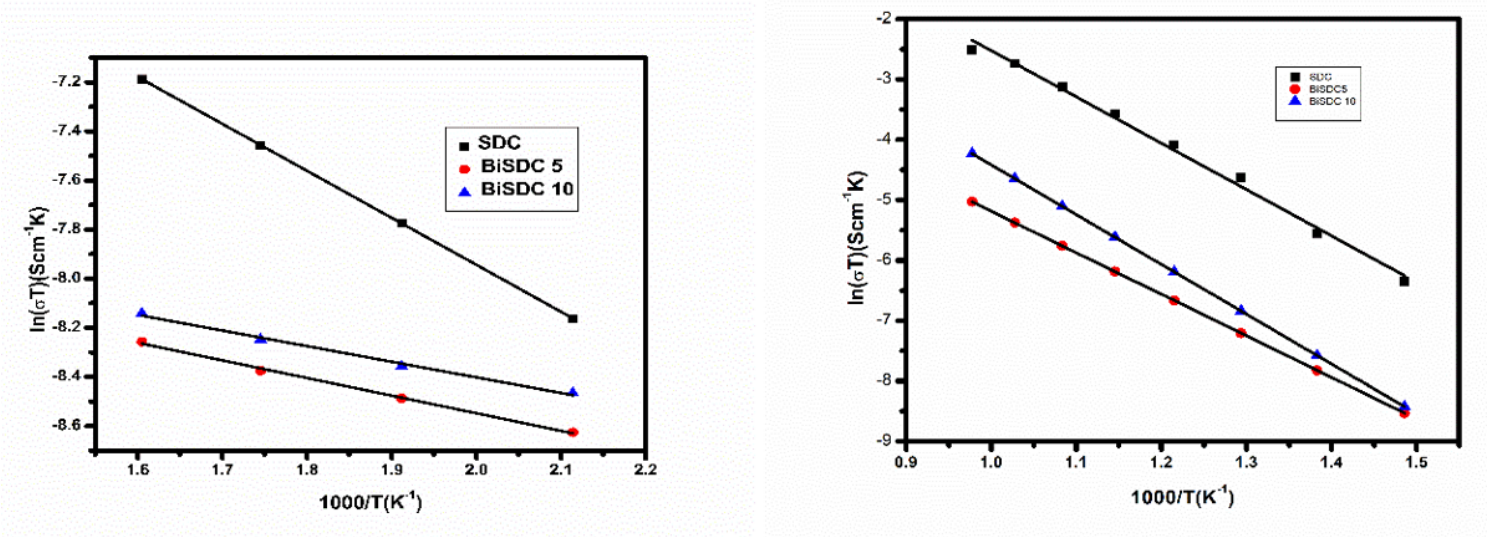

Figure 6

shows the Arrhenius plot of (a).Ce0.8Sm0.2O2-δ,(b) Ce0.8Sm0.15 Bi0.05O2-δ and(c) Ce0.8Sm0.1Bi0.1O2-δ samples at low and high temperature.

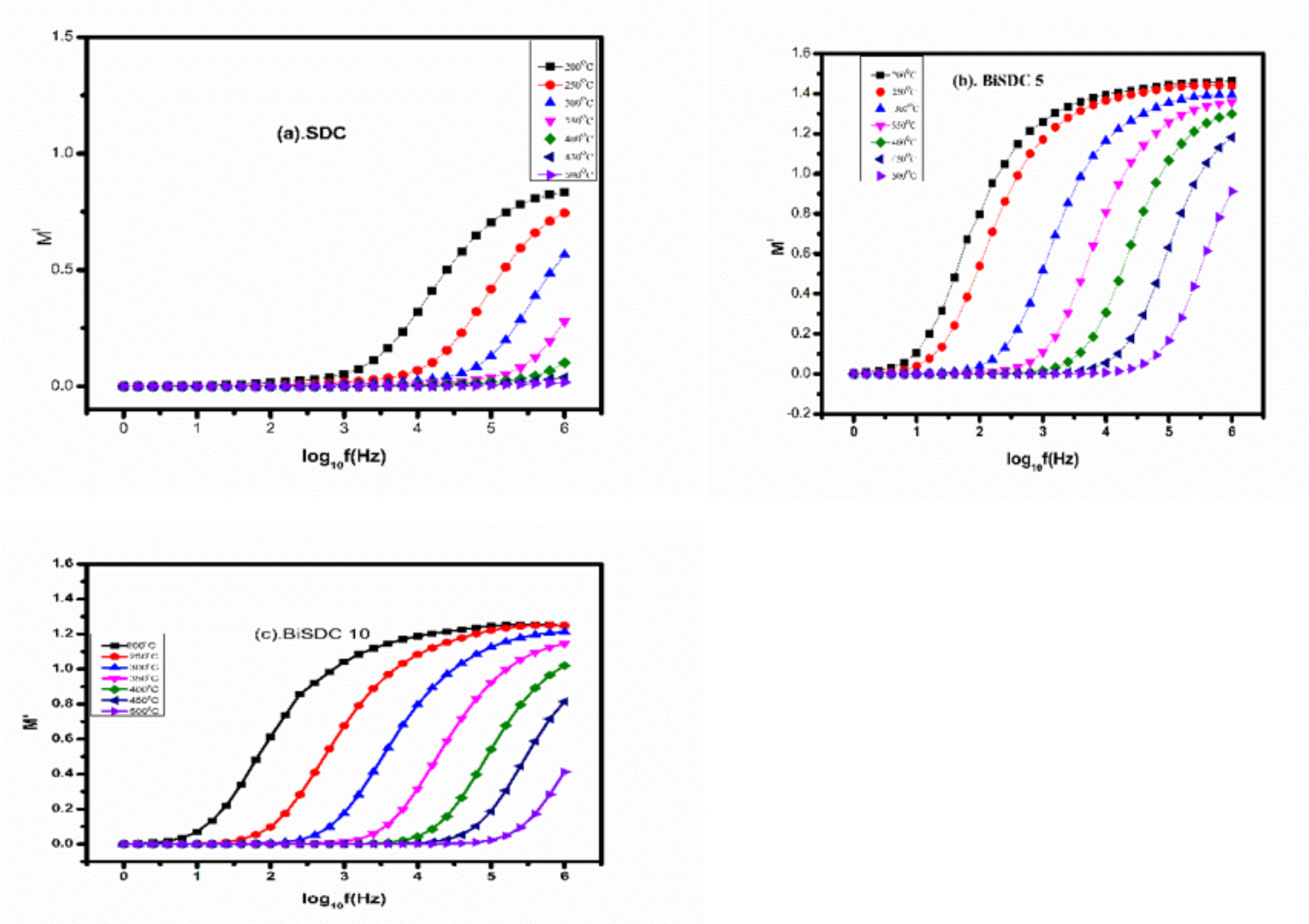

Figure 7

shows the disparity of M' with frequency at selected temperature of 7(a).SDC,7(b). BiSDC 5 and 7(c). BiSDC 10 samples.

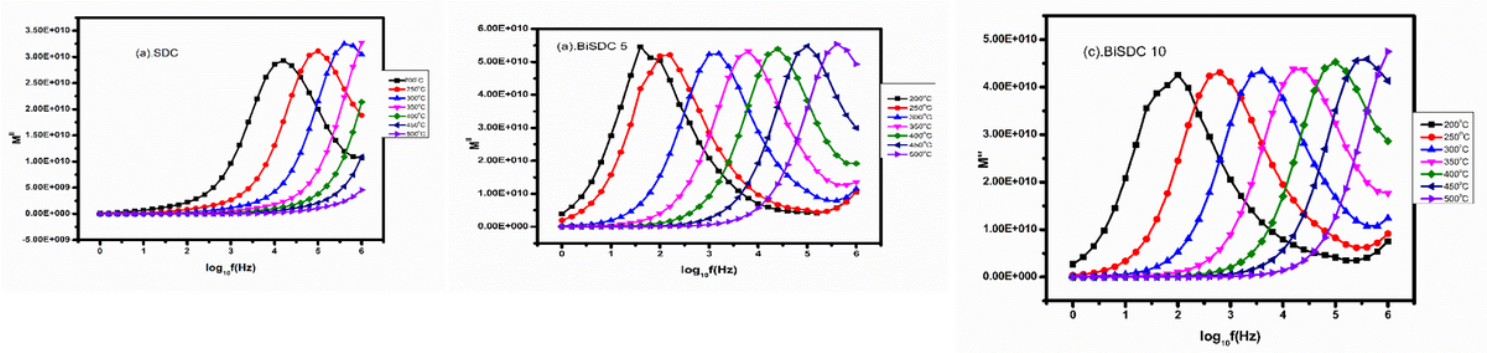

Figure 8

shows the disparity of M" with frequency at different temperatures of 8(a).SDC, 8(b).BiSDC 5 and 8(c). BiSDC 10 samples.